10. K. L. Pierce, R. T. Premont, R. J. Lefkowitz, *Nat. Rev. Mol. Cell Biol.* **3**, 639 (2002).
11. A. M. Spiegel, L. S. Weinstein, *Annu. Rev. Med.* **55**, 27 (2004).
12. H. Ma, M. Yanofsky, E. M. Meyerowitz, *Proc. Natl. Acad. Sci. U.S.A.* **87**, 3821 (1990).
13. H. Ma, *Plant Mol. Biol.* **26**, 1611 (1994).
14. M. G. Mason, J. Botella, *Proc. Natl. Acad. Sci. U.S.A.* **97**, 14784 (2000).
15. M. G. Mason, J. R. Botella, *Biochim. Biophys. Acta* **1520**, 147 (2001).
16. A. M. Jones, S. A. Assmann, *EMBO Rep.* **5**, 572 (2004).
17. S. Plakidou-Dymock, D. Dymock, R. Hooley, *Curr. Biol.* **8**, 315 (1998).
18. G. Colucci, F. Apone, N. Alyeshmerni, D. Chalmers, M. J. Chrispeels, *Proc. Natl. Acad. Sci. U.S.A.* **99**, 4736 (2002).
19. S. Pandey, S. M. Assmann, *Plant Cell* **16**, 1616 (2004).
20. S. M. Assmann, *Science* **310**, 71 (2005).
21. P. Obrdlik et al., *Proc. Natl. Acad. Sci. U.S.A.* **101**, 12242 (2004).
22. X.-Q. Wang, H. Ullah, A. M. Jones, S. M. Assmann, *Science* **292**, 2070 (2001).
23. J. M. Ward, Z. M. Pei, J. I. Schroeder, *Plant Cell* **7**, 833 (1995).
24. S. R. Sprang, *Annu. Rev. Biochem.* **66**, 639 (1997).
25. S. Pandey, J. G. Chen, A. M. Jones, S. M. Assmann, *Plant Physiol.* **141**, 243 (2006).
26. We thank D. Y. Sun for his support; X. W. Deng and J. M. Zhou for their comments and discussion; W. Frommer and P. Obrdlik for making the split-ubiquitin system available; J. Kuala for making the split-YFP system available; J. Chai for his technical assistance and advice for the protein purification; and D. Zhang, Y. Shen, and F. Razem for their suggestions on the ABA binding assay. This work was supported by the Ministry of Science and Technology of China (to L.M., 2003AA210120), National Science Foundation of China for Outstanding Young Scientists (to L.M., 30025024) and the Chinese National Key Basic Research Project (to W.W., 2006CB100100).

Tunability and Noise Dependence in Differentiation Dynamics

Gürol M. Süel,[1] Rajan P. Kulkarni,[2] Jonathan Dworkin,[3] Jordi Garcia-Ojalvo,[4] Michael B. Elowitz[2]*

The dynamic process of differentiation depends on the architecture, quantitative parameters, and noise of underlying genetic circuits. However, it remains unclear how these elements combine to control cellular behavior. We analyzed the probabilistic and transient differentiation of *Bacillus subtilis* cells into the state of competence. A few key parameters independently tuned the frequency of initiation and the duration of competence episodes and allowed the circuit to access different dynamic regimes, including oscillation. Altering circuit architecture showed that the duration of competence events can be made more precise. We used an experimental method to reduce global cellular noise and showed that noise levels are correlated with frequency of differentiation events. Together, the data reveal a noise-dependent circuit that is remarkably resilient and tunable in terms of its dynamic behavior.

Three aspects of genetic circuits control dynamic cellular behaviors: the circuit architecture or pattern of regulatory interactions among genetic elements; quantitative parameter values, such as promoter strengths; and stochastic fluctuations, or "noise," associated with the concentration of cellular components. A fundamental biological question is how these three aspects of genetic circuits combine to determine cellular behavior, its variability, and its potential to evolve (*1*).

Competence in *B. subtilis* is a stress response that allows cells to take up DNA from the environment (*2*, *3*). Differentiation into competence is transient (Fig. 1A) (*4*). The genetic basis for this behavior is a circuit involving *comK* and *comS* (Fig. 1B). The transcription factor ComK is necessary and sufficient for differentiation into competence (*5*, *6*). ComK positively autoregulates its own expression but is degraded by the ClpP-ClpC-MecA protease complex (Fig. 1B) (*7–9*). ComS competitively inhibits this degradation and is repressed in competent cells, forming a negative feedback loop (*4*, *10*, *11*). The circuit operates as an excitable system in which a relatively small perturbation induces a larger and stereotyped response, as occurs with action potentials in neurons, for example (*4*, *12*). Competence events occur only in a fraction of cells and may be driven by noise in underlying circuit components (*4*, *7*, *8*, *13*).

Two key characteristics of competence are its probability of initiation, P_{init}, and the mean duration of transient competence events, τ_{comp} (Fig. 1A). P_{init} denotes the chance per cell division that an individual cell will become competent. Competence events can be quantified by automated time-lapse fluorescence microscopy using fluorescent reporter genes under the control of the ComK-specific *comG* promoter and the *comS* promoter (denoted P_{comG} and P_{comS}, respectively) (*4*).

Two parameters that are expected to affect the behavior of the circuit are the basal expression rates of *comK* and *comS*, denoted by α_K and α_S, respectively (Fig. 1B and Eq. S1). To manipulate these parameters, we chromosomally integrated an additional copy of either *comS* or *comK* under the control of an inducible promoter, denoted P_{hyp}, generating the Hyper-α_S and Hyper-α_K
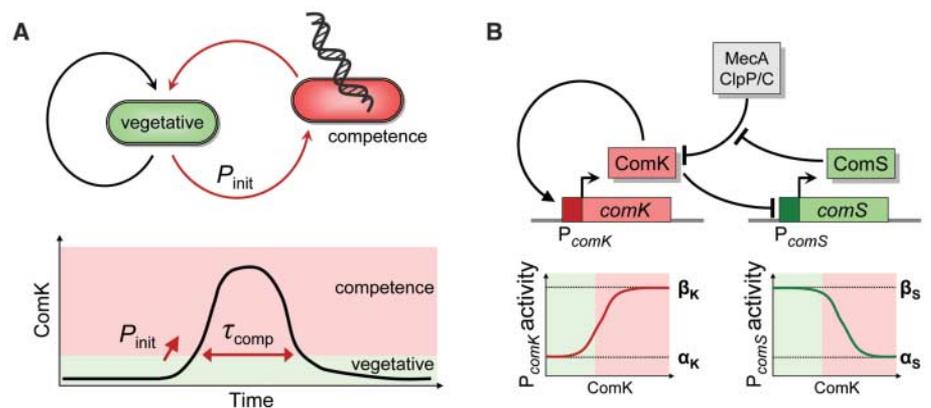

Fig. 1. Competence is a probabilistic and transient differentiation process regulated by a genetic circuit. (**A**) The rate of entering the competent state from the vegetative state is denoted by P_{init}. The amount of time spent in the competent state is denoted by τ_{comp}. The ComK transcription factor concentration is high (pink region) when cells are competent and low (green region) when they are growing vegetatively. (**B**) Map of the core competence circuitry. Key features include positive transcriptional autoregulation of *comK* and a negative feedback loop in which ComK inhibits (possibly indirectly) expression of ComS, which in turn interferes with degradation of ComK. The graphs below the P_{comK} and P_{comS} promoters define parameters used in the text: Expression rates change from α_K to β_K and β_S to α_S respectively, as ComK concentration increases during competence.

[1]Green Center Division for Systems Biology and Department of Pharmacology, University of Texas Southwestern Medical Center, Dallas, TX 75390, USA. [2]Division of Biology and Department of Applied Physics, California Institute of Technology, Pasadena, CA 91125, USA. [3]Department of Microbiology, College of Physicians and Surgeons, Columbia University, New York, NY 10032, USA. [4]Departament de Física i Enginyeria Nuclear, Universitat Politècnica de Catalunya, Colom 11, E-08222 Terrassa, Spain.

*To whom correspondence should be addressed. E-mail: melowitz@caltech.edu

strains, respectively [see Supporting Online Material (SOM) text]. To systematically scan a range of values for α_K and α_S, we made time-lapse fluorescence movies of these strains on media containing different concentrations of the inducer isopropyl-β-D-thiogalactopyranoside (IPTG) (Fig. 2, A and B).
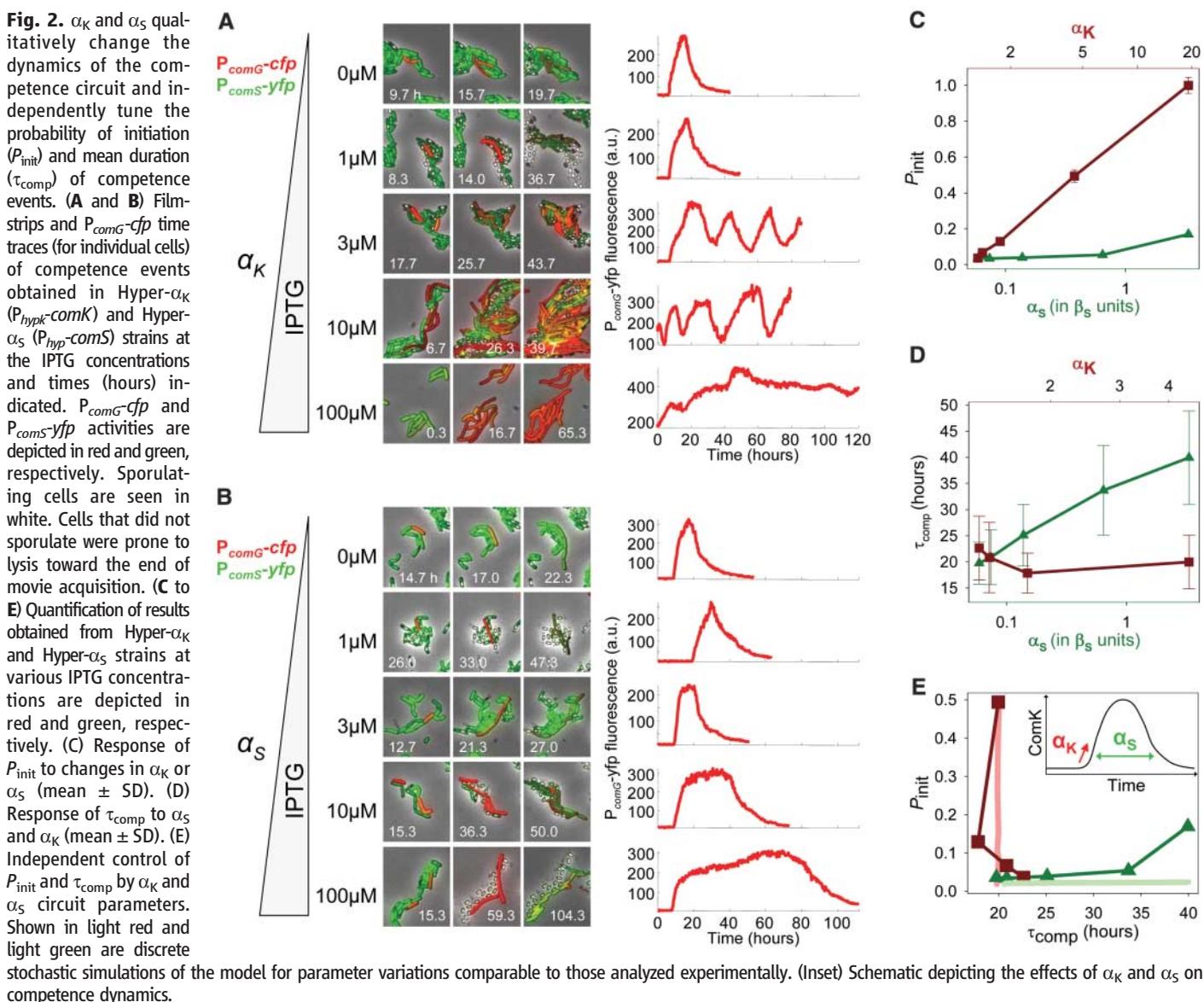
We investigated how α_K and α_S combine to regulate P_{init}. Without IPTG, P_{init} was ~3% in the Hyper-α_K strain, unchanged from its wild-type value. P_{init} increased rapidly with basal *comK* expression (Fig. 2C). Increased expression of *comK* in the Hyper-α_K strain also showed a transition to an oscillatory regime, in which cells repeatedly went in and out of the competent state (Fig. 2A). At α_K ~20 times its wild-type value, α_K^{wt}, all cells entered competence (Fig. 2, A and C). ComS, like ComK, is necessary for competence. However, expression of P_{hyp}-*comS* had a modest effect on initiation, increasing P_{init} to ~20% (Fig. 2C). Thus, P_{init} was predominantly regulated by α_K rather than α_S.

We next considered the effects of the same perturbations on τ_{comp}. Increasing α_K up to ~4.5 × α_K^{wt} caused no increase in τ_{comp} (Fig. 2D). On the other hand, in the Hyper-α_S strain, τ_{comp} increased with increasing expression of P_{hyp}-*comS* (Fig. 2D). Thus, τ_{comp} was predominantly regulated by α_S rather than α_K. Together, these results show that P_{init} and τ_{comp} can be tuned independently by α_K and α_S, respectively (Fig. 2E).

To better understand the effect of *comS* expression on τ_{comp}, we constructed a "6×S" strain in which P_{comS}-*comS* was expressed from a low–copy number plasmid, effectively increasing the activated production rate, β_S, by a factor of 6 over its wild-type value, β_S^{wt}. Unlike P_{hyp}-*comS*, this construct retains the regulation found in the wild-type P_{comS} promoter, including its negligible basal expression rate, α_S^{wt}. Despite this increase in β_S, excitable behavior was maintained, as 53 ± 5% (*n* = 79/151) of competent cells successfully exited the competent state, compared with 61% ± 7% (*n* = 83/136) of wild-type cells. By contrast,

increasing α_S to ~3 × β_S^{wt} in the Hyper-α_S strain prevented the majority of competent cells from exiting [21.3 ± 5% (*n* = 26/122) of competent cells exited (table S4)]. The repressibility of the natural P_{comS} promoter is thus critical for maintaining excitability (4). These results show that excitability can be reliably maintained over a broad range of β_S values.

To better understand independent tuning of P_{init} and τ_{comp}, as well as reliable maintenance of excitability, we developed a model of the core interactions in the competence regulation circuitry (Fig. 1B and SOM text). We used stochastic simulations to account for intrinsic noise of biochemical reactions (14). We also analyzed the corresponding continuous model to determine parameter dependence and to identify a biologically reasonable parameter regime in which the discrete model produced results consistent with experiments. We required the continuous model to remain in the excitable regime as the β_S value was varied by a factor of 6

Fig. 2. α_K and α_S qualitatively change the dynamics of the competence circuit and independently tune the probability of initiation (P_{init}) and mean duration (τ_{comp}) of competence events. (**A** and **B**) Film-strips and P_{comG}-*cfp* time traces (for individual cells) of competence events obtained in Hyper-α_K (P_{hypk}-*comK*) and Hyper-α_S (P_{hyp}-*comS*) strains at the IPTG concentrations and times (hours) indicated. P_{comG}-*cfp* and P_{comS}-*yfp* activities are depicted in red and green, respectively. Sporulating cells are seen in white. Cells that did not sporulate were prone to lysis toward the end of movie acquisition. (**C** to **E**) Quantification of results obtained from Hyper-α_K and Hyper-α_S strains at various IPTG concentrations are depicted in red and green, respectively. (C) Response of P_{init} to changes in α_K or α_S (mean ± SD). (D) Response of τ_{comp} to α_S and α_K (mean ± SD). (E) Independent control of P_{init} and τ_{comp} by α_K and α_S circuit parameters. Shown in light red and light green are discrete stochastic simulations of the model for parameter variations comparable to those analyzed experimentally. (Inset) Schematic depicting the effects of α_K and α_S on competence dynamics.

and we required its stochastic counterpart to generate the observed independent tunability of P_{init} and τ_{comp}. We identified a parameter set that accounts for both maintenance of excitability at high β_S and independent tunability by α_S and α_K. Analysis of the model is described in detail in the SOM text (15).

Within the model, increasing α_K increased the probability that vegetative cells reach the minimum concentration of ComK necessary to initiate competence, explaining the strong effect of α_K on P_{init} (Fig. S5). Increasing α_S, on the other hand, did not raise P_{init} arbitrarily high because initiation of competence is limited by fluctuations in ComK expression (Fig. 2E and fig. S6).

In the model, we also analyzed τ_{comp}. Exit from competence requires ComS to be degraded. When the basal production rate of ComK is less than its activated production rate ($\alpha_K < \beta_K$), ComS degradation, and thus τ_{comp}, is unaffected. On the other hand, as α_S is increased from zero, production of ComS offsets its degradation, prolonging competence duration.

Consistent with experimental results, in the model increasing α_K switches the system from excitable to oscillatory dynamics, further distinguishing α_K from α_S (fig. S3). Increasing α_S takes the system directly from excitability to a bistable regime in which $P_{init} < 1$, but, once initiated, most cells remain trapped in the competent state. This behavior was also observed in experiments where no oscillatory behavior was seen at intermediate α_S values (Fig. 2B).

As in the experiments, cells in the model can become stuck in competence. When the basal production rate of ComK exceeds its activated production rate ($\alpha_K > \beta_K$), ComK levels cannot be reduced in competence, and cells become trapped in the competent state. A similar effect occurs at high α_S values, because a new stable state arises at competence-maintaining concentrations of ComK (Fig. S7). However, in this case, exit of competence remained possible as a result of noise, which destabilizes the newly formed competent state (see Section S1.4 of SOM text). This is consistent with experimental observations showing that, even at the highest induction levels in the Hyper-αS strain, ~20% of cells successfully exited competence.

To explore the effects of perturbing the circuit architecture, we reengineered the competence circuit using Rok, a protein that binds to P_{comK} and represses its expression (16). We inserted a copy of rok under the control of P_{comG}, creating an additional negative feedback loop onto comK (Fig. 3A). In this "CompRok" strain, as expected, P_{init} remained unchanged from its wild-type values (~3%). The mean value of τ_{comp}, on the other hand, was reduced, as was its cell-cell variability. In CompRok, $\tau_{comp} = 13.9 \pm 3.4$ hours (mean ± SD, $n = 30$), compared with $\tau_{comp} = 20.2 \pm 9.9$ hours (mean ± SD, $n = 31$) in wild type (Fig. 3B). This reduction in cell-cell variability showed that the precision of τ_{comp} can be improved over its wild-type value. In the

model (Fig. 3B, insets), this result can be explained as follows: Exit from competence occurs when the absolute number of ComS molecules is very low and the relative size of stochastic fluctuations therefore increases. These effects increase the variability in τ_{comp}. In the CompRok strain,

Fig. 3. Architectural change to the MeKS circuit reduces variability of competence durations (τ_{comp}). (**A**) Competence circuit was rewired to introduce an additional transcriptional negative feedback loop onto comK, generating the CompRok strain. (**B**) Fluorescence time traces, normalized by their maximum value, from P_{comG}-cfp in the CompRok strain or the wild type. Traces have been aligned with respect to time of initiation of P_{comG} expression. For each panel, corresponding discrete stochastic simulations of CompRok and wild-type competence circuits are shown as insets.
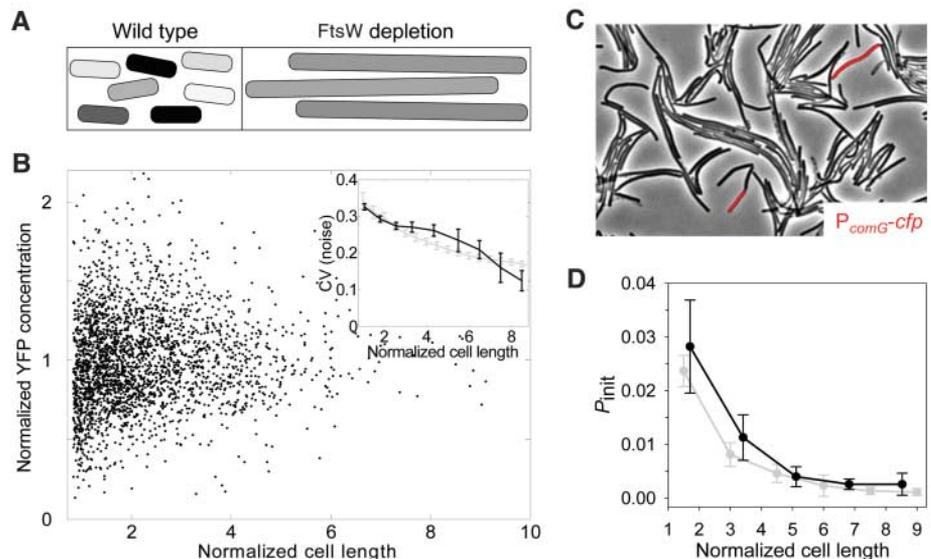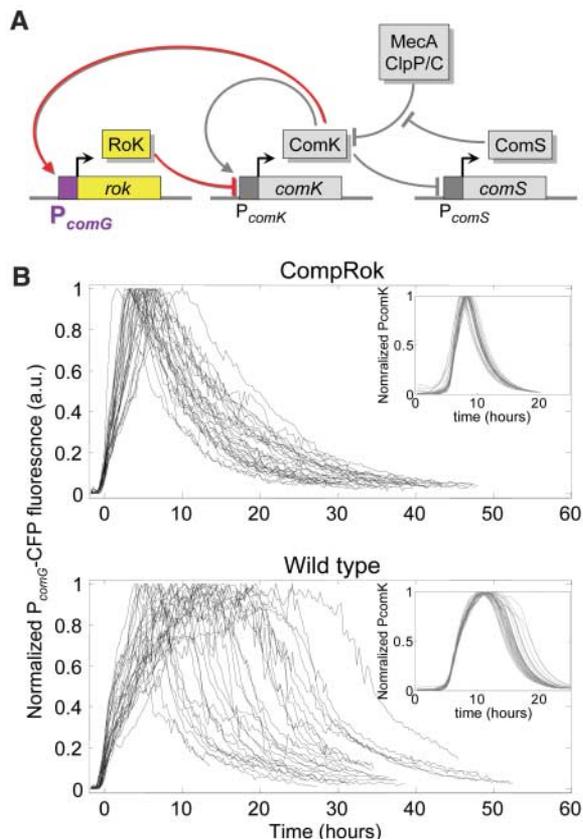

Fig. 4. Noise in gene expression and probability of competence initiation (P_{init}) decreases with increasing cell length. (**A**) Cell-cell variation in gene expression (shades of gray) is expected to decrease in elongated conditional ftsW mutant cells compared with wild-type cells. (**B**) Noise decreases with increasing cell length: Dots represent P_{hyp}-yfp expression (normalized by mean) and length of individual conditional ftsW mutant (Fili-H) cells induced with 5 μM IPTG. (Inset) Coefficient of variation (CV) of P_{hyp}-yfp expression as a function of cell length (black) compared with discrete stochastic model prediction (gray). (**C**) Overlay of phase contrast and P_{comG}-cfp fluorescence (red) snapshots of Fili-SOG cells with increased cell length. (**D**) Experimentally determined P_{init} (black line) drops with increasing cell length consistent with discrete stochastic simulations (gray line). Error bars in (C) and (D) denote one SD. (See S3.4 SOM text for details on calculation of P_{init}.)

however, the additional negative feedback allows exit from competence to occur at higher ComS and Rok concentrations, reducing the sensitivity of τ_{comp} to stochastic fluctuations (fig. S10).

It is not known whether competence initiation is controlled by noise, as in the model. To test the impact of noise on competence initiation, we set out to globally modulate the amount of noise in the cell. We used a *B. subtilis* strain in which the *ftsW* gene, which is necessary for septation, was replaced by an inducible copy. In the absence of inducer, septation was inhibited, resulting in elongated filamentous cells. Each filament was composed of multiple cell units, all sharing cytoplasm. Within a filament, diffusion is expected to effectively average cell contents, reducing noise in gene expression, without affecting mean concentrations of cellular components (Fig. 4A) (*17*). In some bacterial mutants that have elongated filamentous morphologies, cellular growth, nucleoid density, protein expression, and other physiological characteristics appear normal, even though cellular volume is greatly increased (fig. S12) (*18–20*). We integrated an inducible P_{hyp}-*yfp* construct and measured the effect of cell length on cell-cell fluctuations in yellow fluorescent protein (YFP) expression (Fig. 4B). We found that noise does indeed decrease with increasing length (Fig. 4B, inset). A simple model of transcription and translation (*21–24*) that incorporates the continuity of filamentous cell growth produced qualitatively similar results (Fig. 4B, inset, and SOM text). Thus, cell size can in this case be used to modulate gene expression noise.

How does noise affect the probability of initiation of competence? To answer this question, we induced filamentation in the conditional *ftsW* strain at the beginning of, or before, movie acquisition and quantified P_{init} as a function of cell length. We determined length distributions of cells at the moment they initiated competence, as detected by P_{comG} expression (Fig. 4C). As a comparison, we also measured length distributions for noncompetent cells at a similar distribution of times. We plotted the relative fraction of cells that initiated competence at a given length, compared with the total number of cells at that length. The results showed that P_{init} decreased as cells elongated (Fig. 4D and SOM text). A similar decrease in P_{init} was observed in corresponding simulations (Fig. 4D). To test if the reduction in P_{init} could be due to factors other than diminished noise, we examined two promoters, P_{comS} and P_{spo0A}, both strongly regulated under these conditions. Spo0A is a master regulator of sporulation, a competing starvation response, and high concentrations of Spo0A inhibit competence (*3*). Conversely, P_{comS} expression is necessary for competence. Mean expression of both P_{comS} and P_{spo0A} was unaffected by cell length (fig. S17). This supports the idea that gene expression levels are independent of cell length under these conditions and that P_{init} depends on noise.

Noise may play at least three different functional roles in competence. First, noise could be responsible for the observed variability in duration. Second, noise may be necessary to maintain excitability over a wide parameter range, by inducing escape from states of high ComK concentration. Third, noise appears to have a pivotal role in competence initiation (Fig. 4D) and thus should be considered alongside genetic parameters and circuit architecture to comprehensively understand differentiation at the single-cell level.

Quantitative analysis of a genetic system beyond its normal operating regime, including gene expression strengths, circuit architecture, and noise levels, strongly constrains dynamical models. The competence regulation system maintains excitable behavior over a broad range of parameter values. Experimentally, α_K and α_S enable P_{init} and τ_{comp} to be tuned independently, allowing the system, in theory, to adapt to independent selective pressures during evolution. The circuit can also access different dynamic regimes, such as oscillation and bistability, indicating its potential to evolve alternative qualitative behaviors.

References and Notes

1. U. Alon, *An Introduction to Systems Biology: Design Principles of Biological Circuits*. Mathematical and Computational Biology Series, vol. 10 (Chapman & Hall/CRC, Boca Raton, FL, 2006).
2. D. Dubnau, *Annu. Rev. Microbiol.* **53**, 217 (1999).
3. A. D. Grossman, *Annu. Rev. Genet.* **29**, 477 (1995).
4. G. M. Suel *et al.*, *Nature* **440**, 545 (2006).
5. R. M. Berka *et al.*, *Mol. Microbiol.* **43**, 1331 (2002).
6. D. van Sinderen *et al.*, *Mol. Microbiol.* **15**, 455 (1995).
7. H. Maamar, D. Dubnau, *Mol. Microbiol.* **56**, 615 (2005).
8. W. K. Smits *et al.*, *Mol. Microbiol.* **56**, 604 (2005).
9. K. Turgay *et al.*, *EMBO J.* **17**, 6730 (1998).
10. J. Hahn, L. Kong, D. Dubnau, *J. Bacteriol.* **176**, 5753 (1994).
11. M. Ogura *et al.*, *Mol. Microbiol.* **32**, 799 (1999).
12. C. Koch, *Biophysics of Computation* (Oxford Univ. Press, Oxford, 1999).
13. D. Dubnau, R. Losick, *Mol. Microbiol.* **61**, 564 (2006).
14. D. T. Gillespie, *J. Phys. Chem.* **81**, 2340 (1977).
15. The gene circuit shown in Fig. 1B can be described, in a continuous approximation, by two coupled differential equations that govern the dynamical evolution of the concentrations of ComK and ComS proteins, denoted K and S, respectively. The equation for K is $\frac{dK}{dt} = \alpha_k + \frac{\beta_k K^n}{k_k^n + K^n} - \frac{\delta_k K}{1 + K/\Gamma_k + S/\Gamma_s} - \lambda_k K$, where α_k and β_k parameterize the strength of constitutive and autoregulated ComK expression, respectively. The third term models degradation through competitive binding of ComK and ComS to MecA. The final term represents linear degradation of ComK. The equation for S is $\frac{dS}{dt} = \alpha_s + \frac{\beta_s}{1 + (K/k_s)^p} - \frac{\delta_s S}{1 + K/\Gamma_k + S/\Gamma_s} - \lambda_s S$. Here, α_s and β_s measure the strength of constitutive and regulated *comS* expression, respectively. The third and fourth terms represent MecA-mediated and linear degradation, respectively. Other parameters are defined in the SOM text. We have also developed a discrete model of the circuit that incorporates intrinsic noise explicitly. The requirement of independent tunability of P_{init} and τ_{comp} strongly constrains the allowed parameter values and thus the structure of the phase space. The modeling is described in detail in the SOM text.
16. T. T. Hoa *et al.*, *Mol. Microbiol.* **43**, 15 (2002).
17. M. B. Elowitz *et al.*, *J. Bacteriol.* **181**, 197 (1999).
18. F. Ishino *et al.*, *J. Bacteriol.* **171**, 5523 (1989).
19. N. Maki *et al.*, *J. Bacteriol.* **182**, 4337 (2000).
20. F. Tetart *et al.*, *Mol. Microbiol.* **6**, 621 (1992).
21. H. H. McAdams, A. Arkin, *Proc. Natl. Acad. Sci. U.S.A.* **94**, 814 (1997).
22. J. Paulsson, *Nature* **427**, 415 (2004).
23. P. S. Swain, M. B. Elowitz, E. D. Siggia, *Proc. Natl. Acad. Sci. U.S.A.* **99**, 12795 (2002).
24. M. Thattai, A. van Oudenaarden, *Proc. Natl. Acad. Sci. U.S.A.* **98**, 8614 (2001).
25. We thank R. Kishony, B. Shraiman, U. Alon, R. Ranganathan, S. Altschuler, L. Wu, and K. Süel, together with members of the Elowitz laboratory, for thoughtful comments and discussions. This work was supported by grants from NIH (R01 GM079771 to M.B.E. and GM068763 to the Center for Modular Biology), the Searle Scholars Program, the Human Frontiers Science Program, and the Packard Foundation. G.M.S. is supported by California Institute of Technology Center for Biological Circuit Design and the University of Texas Southwestern's Endowed Scholars Program. J.G.O. acknowledges financial support from the Ministerio de Educacion y Ciencia (Spain, project FIS2006-11452) and from the Generalitat de Catalunya.

Temporal Frequency of Subthreshold Oscillations Scales with Entorhinal Grid Cell Field Spacing

Lisa M. Giocomo,[1]* Eric A. Zilli,[1] Erik Fransén,[2] Michael E. Hasselmo[1]*

Grid cells in layer II of rat entorhinal cortex fire to spatial locations in a repeating hexagonal grid, with smaller spacing between grid fields for neurons in more dorsal anatomical locations. Data from in vitro whole-cell patch recordings showed differences in frequency of subthreshold membrane potential oscillations in entorhinal neurons that correspond to different positions along the dorsal-to-ventral axis, supporting a model of physiological mechanisms for grid cell responses.

The entorhinal cortex plays an important role in encoding of spatial information (*1–3*) and episodic memory (*4*). Many layer II neurons of rat entorhinal cortex are grid cells, firing when the rat is in an array of spatial locations forming a hexagonal grid within the environment (*5–7*). The spacing of firing fields in the grid varies with anatomical position of the cell along the dorsal-ventral axis of entorhinal cortex, as measured by distance from the postrhinal border (*5*). Neurons closer to the dorsal border of entorhinal cortex have shorter distances between firing fields. Computa-